Extracting the Salient Features of a Multi-Harmonic Time Response with Closely Spaced Modes

Oliver Khan[1], Brennan Bahr[2], Nandan Shettigar[3], Aabhas Singh[4], Robert J. Kuether[4], Matthew S. Allen[5], Matthew R. W. Brake[6], Benjamin Moldenhauer[4], Daniel Roettgen[4], Kevin Dowding[4]

[1]Undergraduate Student, University of Southern California, Department of Aerospace and Mechanical Engineering
[2]Undergraduate Student, Brigham Young University, Department of Mechanical Engineering
[3]Graduate Student, Texas A&M University, Department of Mechanical Engineering
[4]Sandia National Laboratories*
[5]Professor, Brigham Young University, Department of Mechanical Engineering, matt.allen@byu.edu
[6]Associate Professor, Rice University, Department of Mechanical Engineering

Abstract

Joints in structures exhibit hysteresis and energy dissipation characterized by a softening of the joint stiffness and an increase in the damping. These properties are often characterized on a modal basis by applying the Hilbert transform to extract the effective natural frequency and damping of a mode as a function of amplitude. The Hilbert transform assumes that a single harmonic is present, so a response must be filtered to isolate a single mode before it can be applied. During the filtering process, data are often lost to avoid spurious end effects, particularly when a response does not fully decay. Direct Time Fitting mitigates this issue by splitting the time response into small segments and directly fitting the multi-harmonic signal with damped sinusoids at the natural frequency of each mode. While this works for modes with natural frequencies that are well-separated, there is growing interest in characterizing closely spaced modes that arise in structures with symmetry. These problems are challenging for the optimization in Direct Time Fitting and filter-based methods such as the Hilbert transform because it is difficult to separate the frequency and damping of two modes if their frequencies are close. To address this issue, three system identification methods were evaluated on their ability to capture the natural frequency and damping curves of closely spaced modes. These methods were the Hilbert transform, Direct Time Fitting, and a data-driven reduced-order modeling approach based on spectral submanifold (SSM) theory. Their performance was quantified on two mono-harmonic and two multi-harmonic signals with known analytical natural frequency and damping solutions before being applied to unforced experimental data from a symmetric metal airplane structure.

*Sandia National Laboratories is a multimission laboratory managed and operated by National Technology and Engineering Solutions of Sandia, LLC., a wholly owned subsidiary of Honeywell International, Inc., for the U.S. Department of Energy's National Nuclear Security Administration under contract DE-NA-0003525. SAND2024-13625C

Keywords: Signal Processing, Time Fitting, Closely-Spaced Modes, Backbone Curves, Nonlinear Vibrations

1 Introduction

Nonlinear system identification is the process to determine a model that can describe the salient features of a nonlinear dynamical structure. Vibrating structures are described through the frequency of the modes at which they resonate and the energy dissipation/damping of those modes. For signals produced by linear systems, the frequency and damping of each mode are independent of the response amplitude and can be captured through the fast Fourier transform (FFT). However, in nonlinear systems, the modal parameters can effectively change through time with respect to response amplitude, and as a result, the Fourier transform produces a smeared representation of the system dynamics in the frequency domain. A number of nonlinear system identification methods have been proposed [1] [2] to tackle various nonlinearities such as geometric, inertial, material, and hysteretic nonlinearity among others, but there has been varying degrees of success using them with hysteretic systems, such as structures with friction in mechanical joints.

One approach for system identification is to use data to derive a nonlinear differential equation, or reduced-order model (ROM), that can approximate a structure's response to different initial conditions and forcing. The state-space spectral submanifold (SSM) method has gained attention for its use of invariant manifolds that approximate nonlinear trajectories more accurately than linear eigenspaces [3]. The SSM approach is also beneficial as ROMs can be made more accurate without increasing their dimension. The standard procedure for increasing model accuracy with SSMs is to keep the dimension the same, but include higher order polynomial terms that capture more complex nonlinearities, as is discussed further in Section 2.3. This allows for 3-7 dimensional ROMs to describe finite element structures with more than 10^5 degrees of freedom [4].

Another approach for system identification is to approximate a response as a sum of modes with amplitude-varying natural frequency and damping. If this approach is taken, then there are several mono-harmonic methods that can be applied to find the damping and natural frequency of each mode. These include the Hilbert transform [5] and Restoring Force Surface (RFS) method [6], as well as the time fitting approach by Goyder and Lancereau [7] that fits a damped sinusoid to short intervals of an SDOF response. When applying these methods to an MDOF response, a multi-harmonic signal must be separated into mono-harmonic components using a filter. Current filtering methods include the modal (or spatial) filter [8] constructed from a matrix of mode shapes, bandpass filters that do not require knowledge of mode shapes, and alternative methods, such as empirical mode decomposition (EMD) and empirical Fourier decomposition (EFD), which break signals up into a sequence of narrow-band components [9]. While these mono-harmonic techniques can provide insight into the frequency and damping trends of individual modes, they can yield spurious end effects in the natural frequency and damping solutions and may miss additional nonlinear phenomena such as modal interactions.

The shortcomings of filters have encouraged the development of multi-harmonic methods that extract natural frequency and damping directly from a MDOF response without any filtering. One such technique is the Direct Time Fitting method, which was introduced by Singh and Allen [10] as an extension of the mono-harmonic time fitting method by Goyder and Lancereau [7]. In Direct Time Fitting, a multi-harmonic time response is split into short intervals, and a summation of decaying sinusoids with constant frequencies and damping ratios are fit within each interval using a nonlinear least squares procedure. Since all modes can be fit simultaneously, this method does not require any modal decomposition to be applied beforehand.

While spectral submanifold reduced-order models (SSM-ROMs) [3], the Hilbert transform, and Direct Time Fitting [10] have been applied to systems with modes that have distantly spaced natural frequencies, they have yet to be tested systematically on closely spaced modes. Such modes with closely spaced frequencies can pose several challenges to nonlinear system identification. When modes are closely spaced, their frequency and damping characteristics may overlap, making it difficult to distinguish between individual modes, especially the damping of each mode. Furthermore, there is limited resolution between test system time response outputs which may make it challenging to distinguish between closely spaced modes in the frequency domain. Lastly, there can be interactions between modes that affect their individual responses. This coupling occurs when the excitation of one mode causes a transfer of energy that perturbs another mode [11].

The contribution of the present work is to compare the performance of the Hilbert transform, Direct Time Fitting, and SSM-ROMs in extracting the damping ratios and natural frequencies of closely spaced modes as a function of physical or modal amplitude. In Section 2, these methods are explained in more detail, and their accuracy on four signals with known analytical solutions is then given in Section 3. Their performance on an experimental wing structure with no analytical solution is presented in Section 4, and conclusions are given in Section 5. Although modal coupling can be a key factor to consider when analyzing closely spaced modes [12], this study focuses on responses with uncoupled modes in order to test the limitations of each method in this simpler scenario. Future work will consider responses with coupled modes in more detail.

2 Methods

The Hilbert transform, Direct Time Fitting, and spectral submanifold (SSM) methods were chosen for this project because they each had distinct capabilities that could be applied in different sets of scenarios. The Hilbert transform technique was designed with the specific purpose of extracting natural frequency and damping curves of mono-harmonic signals. The Direct Time Fitting method was also specifically designed to compute frequency and damping, but could accept multi-harmonic or mono-harmonic inputs. In contrast, the SSM method was made as a general tool to predict how a system would respond to different initial conditions and periodic forcing [3]. Although SSM-ROMs could be computed from multi-harmonic inputs with coupled modes [13], this study only considered ROMs from mono-harmonic inputs to increase the accuracy of the resulting frequency and damping curves. When the Hilbert transform or SSM method needed to analyze a multi-harmonic response, that signal was first decomposed into a sequence of mono-harmonic signals using at least one of three filtering techniques, reviewed in Section 2.1.

2.1 Filtering Techniques

Three filtering techniques were employed to decompose multi-harmonic responses into a set of mono-harmonic components for further analysis by the Hilbert transform or SSMs. The first type of filter considered was a 3rd order Butterworth bandpass filter, implemented with MATLAB's *filtfilt* function for forward and reverse filtering to preserve the phase of the signal. One benefit of this method was that it could be used on a single time series without knowledge of the system's mode shapes. The Butterworth filter could also be applied on existing mono-harmonic signals to remove some of the noise present, which made it a useful post-processing tool for other decomposition methods. The second type of filter was the modal filter [8]. This filter works by converting local physical displacements, $\mathbf{x}(t)$, into global modal displacements, $\mathbf{q}(t)$, using the equation

$$\mathbf{q}(t) = \Phi^{-1}\mathbf{x}(t), \tag{1}$$

where Φ is the mode shape matrix. In some cases, when there are a large number of DOFs, it is not practical to calculate all of the mode shapes of the system. This results in a mode shape matrix that is not square. When this happens, the Moore-Penrose pseudoinverse Φ^{+} is used in place of the matrix inverse.

The third filtering technique considered was empirical Fourier decomposition (EFD) leveraging an iterative sifting method in conjunction with the Fourier spectra of a signal to characterize a nonlinear signal into sub-signals termed intrinsic mode functions (IMF) [14]. The sifting method involves identifying the local minima and maxima of a signal where the time resolution of the local optima corresponds to the extracted frequency range of the signal. Hence a combination of Fourier techniques and sifting methods such as empirical mode decomposition (EMD) [15] reveals the spectral evolution of a signal by finding sub-signals. The extracted sub-signals, or IMFs, contain a lower number of harmonics and can be converted into relatively mono-harmonic signal which enables the output of EFD be of potential use and value for the assumption needed in the Hilbert transform. The range and resolution of the sub-signals can be tuned for this data-driven approach. Hence, with appropriate parameter-tuning, this method can decompose a multi-harmonic signal into a series of intrinsic mode functions that are damped and mono-harmonic. These IMFs are also ordered by their frequency band range in the original signal. Importantly, these are the inferred underlying sources for the observed, detected origin signal. Thus, this is a purely mathematically driven estimation of the modes that make up a signal. However, the degree of reliability of these iterative sets of information preserving transformations must be investigated in terms of representing physical modal features. This can help gauge if the tool is useful for further nonlinear system identification. Although EFD was designed specifically to handle multi-harmonic responses, one question of interest in this work was whether EFD could be applied to a mono-harmonic signal, and return that same mono-harmonic signal back. This was a basic property that was expected to hold for any modal decomposition method. Therefore, EFD was applied to mono-harmonic responses in this work to verify that EFD would indeed return one dominant IMF that corresponded to the input signal.

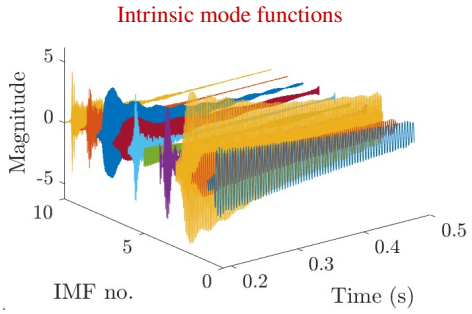

Figure 1: Example output of empirical Fourier decomposition (EFD) showing intrinsic mode functions (IMFs) that make up a multi-harmonic signal.

2.2 Hilbert Transform

The Hilbert transform is a technique that extracts the damping and natural frequency curves of a mono-harmonic signal [5] [16]. This method works by considering an input signal $y(t)$ as the real part of a complex signal

$$Y(t) = y(t) + i\tilde{y}(t). \tag{2}$$

The imaginary component $\tilde{y}(t)$ is defined to be the Hilbert transform of the original signal,

$$\tilde{y}(t) = \mathcal{H}[y(t)] = \frac{1}{\pi t} * y(t) = \frac{1}{\pi}\int_{-\infty}^{\infty} \frac{y(\tau)}{t-\tau} d\tau, \tag{3}$$

which has a 90° phase shift relative to $y(t)$ [17]. Once the complex signal $Y(t)$ is obtained, it is decomposed as an amplitude $A(t)$ and phase $\psi(t)$,

$$A(t) = \sqrt{y(t)^2 + \tilde{y}(t)^2}, \tag{4}$$

$$\psi(t) = \arctan\left(\frac{\tilde{y}(t)}{y(t)}\right). \tag{5}$$

The definition of the phase angle is what makes the Hilbert transform a mono-harmonic method, since oscillations at multiple frequencies cannot generally be determined by a single phase variable. After defining the instantaneous frequency to be $\omega(t) = d\psi/dt$, the natural frequency $f_n(t)$, in Hz, is calculated using

$$f_n(t) = \frac{1}{2\pi}\sqrt{\omega^2 - \frac{\ddot{A}}{A} + \frac{2\dot{A}^2}{A^2} + \frac{\dot{A}\dot{\omega}}{A\omega}}. \tag{6}$$

The damping ratio is similarly computed to be

$$\zeta(t) = \frac{1}{2\pi f_n}\left(-\frac{\dot{A}}{A} - \frac{\dot{\omega}}{2\omega}\right). \tag{7}$$

When this procedure is implemented in MATLAB, the amplitude $A(t)$ is determined by fitting an amplitude envelope of the original signal with a smoothing spline curve, and the phase $\psi(t)$ is similarly fit using a spline. This smoothing is necessary as the numerical implementation of the Hilbert transform generally introduces nonphysical ringing in the envelope that needs to be removed. For the signals studied in this work (which are detailed in Section 3), 10 or fewer knots were used when constructing the spline because otherwise, the spline would over-fit and have nonphysical oscillations. A general schematic of the MATLAB workflow, which shows a typical region for spline fitting, is shown in Fig. 2.

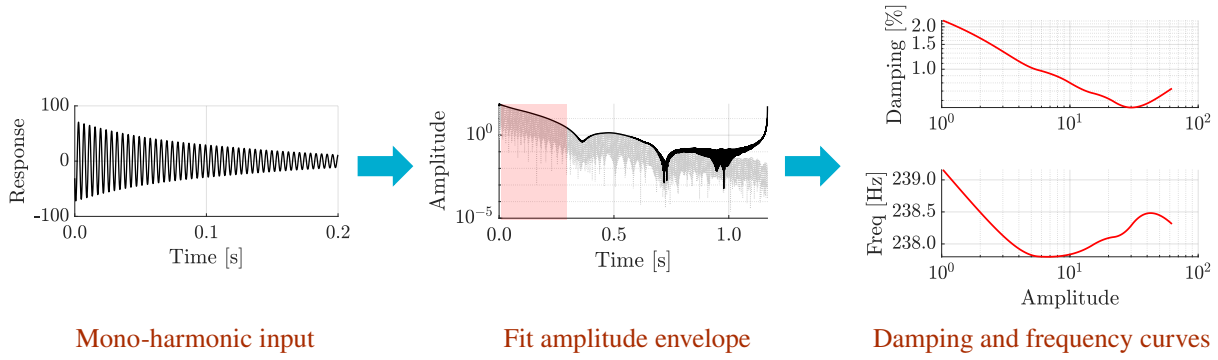

Figure 2: Overview of the Hilbert transform implementation in MATLAB. The region where the amplitude envelope is fit with a spline curve is shown in red. The small fluctuations in the damping and natural frequency near an amplitude of 10^1 can be mitigated by fitting the amplitude envelope with a first or second order spline without any curvature, instead of the cubic spline used here. The damping and natural frequency in the curves to the right also keep increasing at low amplitudes because the signal shown in these plots is not actually mono-harmonic, and has a beat at $t \approx 0.4$. Such beating can occur due to deficiencies in the filters used to pre-process closely spaced modes.

2.3 Spectral Submanifold Reduced-Order Models

Spectral submanifolds (SSMs) are the unique, smoothest nonlinear continuations of linear eigenspaces in phase space [18]. They have been proven to exist under fairly general non-resonance conditions (for details, see [18]), and they are useful structures for reduced-order modeling because phase space trajectories are attracted onto them. In the years since their existence and uniqueness were established, SSM-ROMs have been applied to a growing number of problems inside and outside of structural dynamics. These problems have included high-dimensional finite element models [13], experimental measurements from a half Brake-Reuß beam [19], fluid flow past a circular cylinder [3], and an underwater flag moving chaotically with an impinging freestream [20]. Most of these studies were conducted using the open-source MATLAB package SSMLearn, which can compute ROMs from trajectory data [3].

The reduced-order models in the present study were also constructed using SSMLearn. The input data was just one displacement vs. time trajectory, $x(t)$, from a freely decaying response. Although the variable $x(t)$ represents a physical displacement, modal responses $q(t)$ were also supplied to SSMLearn to evaluate its performance on data from a modal or bandpass filter. After being

supplied with a displacement vs. time signal, SSMLearn computed an observable vector, $\mathbf{y}(t)$, using between 50 and 100 time-delayed versions of the displacement response. The precise number of time-delay coordinates was a user-defined parameter, and needed to be high in this study to create the most accurate ROM possible. Since $x(t)$ was an exponentially decaying vibration signal, the observable trajectory $\mathbf{y}(t)$ spiraled toward an equilibrium point at the origin, $\mathbf{y} = \mathbf{0}$. The next step was to determine the SSM dimension required for constructing the desired ROM. Since this investigation was concerned with 1 DOF ROMs, only 2D SSMs were required.

Then using the observable trajectory $\mathbf{y}(t)$ and the supplied manifold dimension, SSMLearn computed the SSM as an invariant manifold tangent to the plane spanned by the leading eigenvectors of the linearized dynamics at the origin. A schematic image showing an SSM as a nonlinear continuation of an eigenspace is shown in Fig. 3. In this figure, the red dot represents a fixed point at the origin, the purple plane represents an eigenspace, and the green manifold is the SSM. The black curve in Fig. 3 represents a low-amplitude trajectory in the observable space spiraling toward the origin along the SSM.

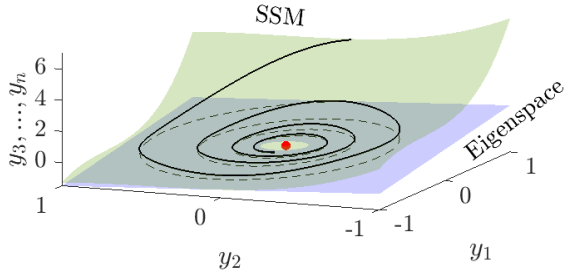

Figure 3: Visualization of a 2D SSM as a nonlinear continuation of an eigenspace in the observable phase space with $\mathbf{y}$ coordinates. The nonlinear dynamics restricted to the SSM are denoted by the solid curve, while the linearized dynamics along the eigenspace are represented by the dashed curve. The red dot is a fixed point at the origin.

Once the SSM is determined, the reduced dynamics along it are expressed in terms of a polynomial system of differential equations of the form

$$\dot{\mathbf{u}} = R_0\mathbf{u} + \sum_{|\mathbf{k}|\geq 2}^{n_{\text{model}}} R_{\mathbf{k}}\mathbf{u}^{\mathbf{k}} \tag{8}$$

where $\mathbf{u}$ is a vector of reduced coordinates, R_0 is a matrix representing the linear part of the reduced-order model, $\mathbf{k}$ is a multi-index, and $R_{\mathbf{k}}$ is a matrix of coefficients for the nonlinear dynamics of polynomial order $|\mathbf{k}|$. The overall polynomial order of the ROM, represented by n_{model} is an important user-defined parameter. In this study, reduced-order models of order 9-11 were considered because they were accurate enough to approximate non-polynomial dynamics over short intervals, but also low enough to mitigate over-fitting issues. After finding the reduced dynamics, a user can resent the ROM in normal form style. This was a key step in this work because SSMLearn needs a normal form representation of the reduced dynamics to determine the amplitude-dependent natural frequency and damping ratio of the modes included in the ROM. For more details on the computations in SSMLearn, see [3].

2.3.1 Multiple Reduced-Order Models for Split Response Signals

The input data for SSMLearn were displacement responses that started at large amplitudes and then decayed to smaller amplitudes (as detailed Sections 3-4). Two challenges arose in computing ROMs for these responses because SSMLearn was not used as it was originally intended. First, SSMLearn was designed to fit SSMs on low-amplitude data and the literature does not advocate fitting SSMs to high-amplitude data, where higher-order transient dynamics can be active [3] . Since SSMs in this study were fit to the entirety of a response, including the high-amplitude portions, the reduced-order models obtained from SSMLearn could have decreased accuracy at low amplitudes. Another problem with the implementation of SSMLearn in the present work was that SDOF reduced-order models were computed for SDOF responses, as outlined in Section 3. Since these responses had non-polynomial nonlinearities that SSMLearn had to approximate with polynomials, there were further inaccuracies that came with using the high-amplitude data when fitting the SSM.

Since SSMLearn was being applied in a way that was not supported by previous literature [3], the frequency and damping curves obtained in this work appeared to become overly flat, and diverged from analytical solutions at small amplitudes. To increase the accuracy of these SSM-ROMs, attempts were made to adjust the regression weighting when calculating the reduced dynamics. However, these efforts resulted in unphysical models with fluctuating natural frequency and damping at large amplitudes. These results persisted even after a genetic algorithm was run to find the regression weightings that minimized the square

norm error between an input signal and the resulting ROM in the time domain. Therefore, an alternative remedy was devised. This temporary solution, designed purely to increase the accuracy of damping and natural frequency curves, was called the "split SSM method" or "sSSM" for short. This method first computed a ROM for the entirety of a response, but then found another ROM for just the low amplitude portion. If needed, a third ROM was determined for even smaller amplitudes where the second ROM became inaccurate. The process continued until a series of ROMs captured the nonlinearity in the frequency and damping at the smallest amplitudes. An example of this technique is shown in Fig. 4. Since this sequence of ROMs could not be integrated on initial conditions, the split SSM method was considered a useful trick to produce more accurate backbone curves, but not a long-term alternative to traditional SSM-ROMs.

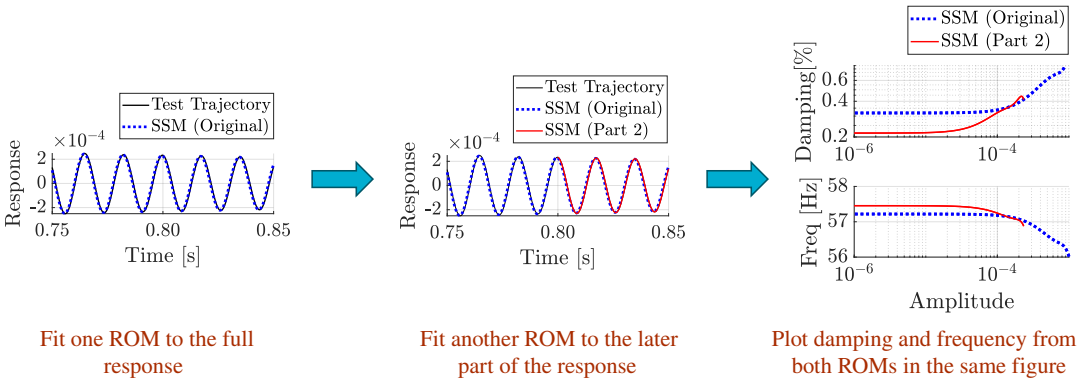

Figure 4: Schematic showing how an SSM-ROM can have improved accuracy when the SSM is fit just to low-amplitude data (SSM Part 2) instead of the entirety of a response. The left plot shows one ROM (blue) fit to a given response and the middle plot shows another ROM (red) fit to the later part of the trajectory. The final plot shows the additional nonlinear behavior that is captured by the second ROM at low amplitudes. The left and middle plots are also zoomed-in to show precisely where the second ROM is fit to the later portion of the decaying signal.

2.4 Direct Time Fitting

The Direct Time Fitting method, also referred to as DTimeFit in this work, was proposed by Singh and Allen [10] as an expansion of the work previously done by Goyder and Lancereau [7] to find the natural frequency and damping of multiple uncoupled nonlinear modes simultaneously. This method takes a signal $y(t)$ with M distinct modes, and divides it into multiple overlapping sections. The windows are narrow enough to assume that the signal in each section is made from a superposition of M linear responses that oscillate at frequencies corresponding to the modes active in the signal. This assumption allowed the response in each window to be fit to the model curve,

$$y_{\text{fit}}(t) = \sum_{i=1}^{M} e^{-\beta_i t}[A_i \cos(\alpha_i t) - B_i \sin(\alpha_i t)], \tag{9}$$

where α_i and β_i are simplified frequency and damping terms, and A_i and B_i are amplitude terms for the i-th mode. If N is the number of time steps included in a window, then the model curve given by Eq. 9 is determined by minimizing the cost function

$$J[y_{\text{fit}}] = \sum_{j=1}^{N} |y_j - y_{\text{fit}}(t_j)|^2 \tag{10}$$

with respect to the parameters α_i, β_i, A_i, and B_i. In Eq. 10, y_j is defined to be the value of the input signal at the discrete time t_j. This process is then repeated throughout the length of the signal, with each subsequent window slightly overlapping the previous window to capture small changes in frequency and damping. After finding y_{fit}, the instantaneous frequency for the i-th mode in each window is calculated to be

$$\omega_{n,i} = \sqrt{\alpha_i^2 + \beta_i^2}, \tag{11}$$

and the instantaneous damping for the i-th mode in each window is defined as

$$\zeta_i = \frac{\beta_i}{\sqrt{\alpha_i^2 + \beta_i^2}}. \tag{12}$$

The natural frequency and damping from all of the windows are then plotted with respect to amplitude to visualize nonlinear shifts that occurred in the signal, as shown in Fig. 5. This process is also sped up by supplying the gradient of Eq. 9 to MATLAB when minimizing the cost function J. Finding the gradient of the cost function is quite complicated due to the dependence of A_i and B_i on α_i and β_i. For more information on how the gradient is calculated, see [17].

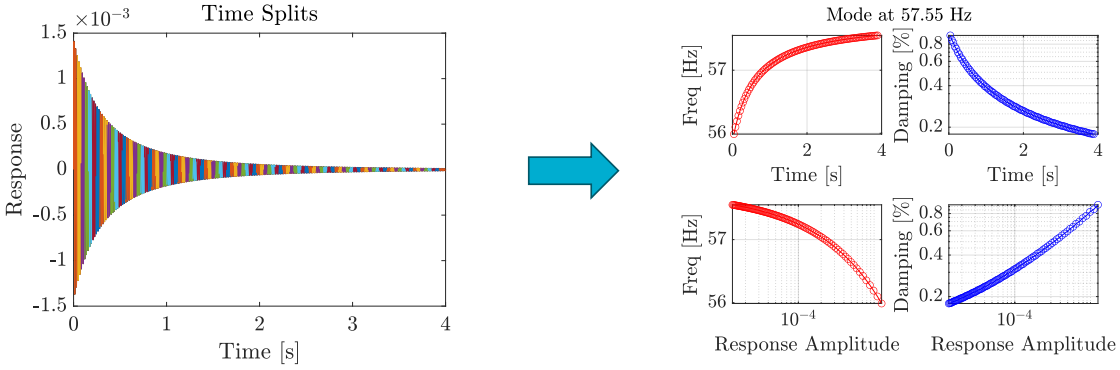

Figure 5: Direct Time Fitting produced natural frequency and damping curves by splitting a response into small windows and fitting a superposition of damped sinusoids in each window. These sinusoids from all of the windows formed a piecewise representation for each mode in the input signal. Backbone curves are then obtained by plotting the frequency and damping for each mode across all of the windows.

3 Comparison of Methods

To compare the accuracy and computational costs of the methods outlined in Section 2, four signals with analytical damping and natural frequency solutions were generated to be analyzed by each of the methods. The damping ratios and natural frequencies in these responses are included in Table 1. These signals were denoted as steps 0-3, where step 0 was the simplest type of response and step 3 was anticipated to be the most challenging to analyze. As the FFTs in Fig. 6 demonstrate, the signals had increasing levels of nonlinearity from step 0 to step 3.

Table 1: Analytical signals used for verification

Comparison Step	Response	Damping [%]	Natural Frequency [Hz]
0	1 Mode, Linear	0.20	25.0
1	1 Mode, Nonlinear	$0.18 - 0.95^{a,b}$	$55.9 - 57.5$
2	2 Distant Modes, Nonlinear	$0.18 - 0.95$ $0.20 - 0.80$	$55.9 - 57.5$ $155.0 - 158.5$
3	2 Close Modes, Nonlinear	$0.18 - 0.95$ $0.20 - 0.80$	$55.9 - 57.5$ $60.4 - 61.6$

[a] For cells that extend across two lines, the first line pertains to mode 1, and the second line to mode 2.

[b] Approximate min/max damping and natural frequency values are given for nonlinear signals.

The first of the signals, deemed Step 0, was a SDOF linear response,

$$y = e^{-\zeta\omega_n t}[\sin(\omega_d t) + \cos(\omega_d t)], \tag{13}$$

where $\omega_n = 2\pi f_n$ was the natural frequency and $\omega_d = \omega_n\sqrt{1-\zeta^2}$ was the damped frequency. Since step 0 was a linear response, the natural frequency and damping ratio remained constant with respect to amplitude. Fortunately, each method was able to find the frequency and damping of this signal, as shown in Fig. 7. The exception to this was the Hilbert transform used on the first intrinsic mode (IMF) function obtained from EFD (denoted EFD-Hilbert), which did not capture the correct

damping ratio at amplitudes less than 0.1 and amplitudes greater than 0.5. The reason for this disagreement could be that the EFD data was inadvertently adding spurious transient features to the signal, and suggests a shortcoming of this method which must be taken into account in future applications. Another possible explanation for the inaccuracy was that the spline curve used to compute the damping ratio had too many knots, and thus did not eliminate the ringing caused by the numerical Hilbert transform. Consequently, it is a topic of future studies to more thoroughly investigate the mutual combination of EFD and the Hilbert transform.

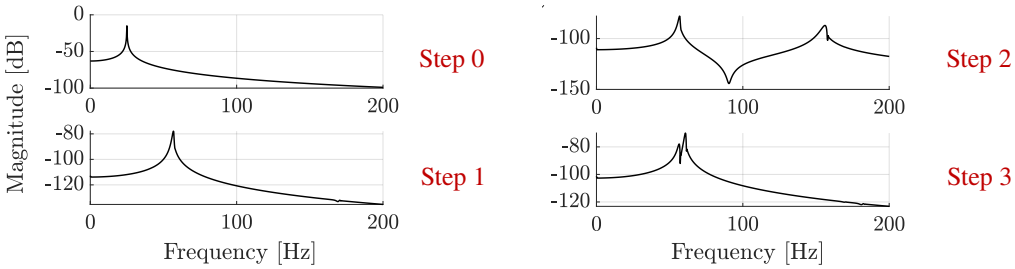

Figure 6: FFTs of the verification signals. Steps 0 and 1 were mono-harmonic, while steps 2 and 3 had two modes.

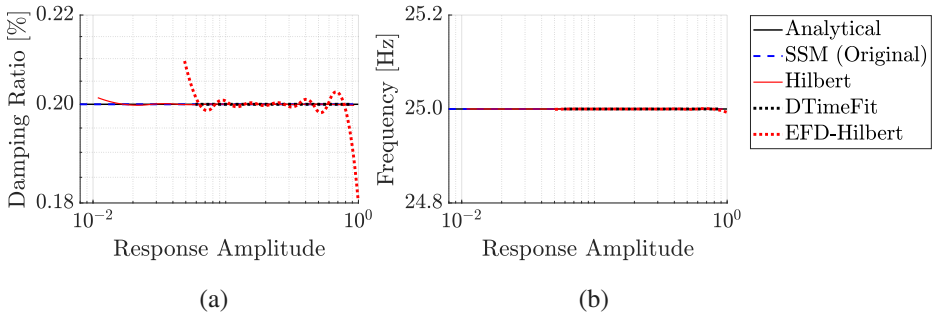

Figure 7: Step 0 damping ratio (a) and natural frequency (b) computations for the 1 DOF linear response. All methods performed well except the "EFD-Hilbert" approach, which produced spurious ringing in the damping ratio. The "SSM (original)" method computed natural frequency and damping ratio from a single ROM, and the "Hilbert" method applied the Hilbert transform to the mono-harmonic response without application of EFD. The response amplitude shown in this plot is the physical amplitude.

The second verification signal was generated using a SDOF oscillator with a four-parameter Iwan element inserted in parallel with the oscillator's spring. The Iwan element is a mathematical model that captures nonlinear behaviors due to friction. It was chosen to add nonlinearity to the signals because it had a closed-form solution, which allowed for the amplitude dependent frequency and damping to be calculated. For more information on the Iwan element, see [21]. Although nonlinearity was introduced into this signal due to the Iwan element, the system still only consisted of a single mode. This meant that each method could be applied directly to the signal without first filtering the response. The only exception was the EFD-Hilbert method, which still applied EFD to the mono-harmonic input to verify that the leading IMF would be the same as the original signal. As seen in Fig. 8, each method was able to extract the amplitude dependent frequency and damping from the response of step 1 at high amplitudes. The SSM-ROM (SSM Original) that was fit to the entire response struggled at low amplitudes because the regression in SSMLearn was focused on fitting the whole time response, which caused the low-amplitude part to become less accurate. Accuracy at low amplitudes was later improved when a ROM was fit to just the lowest amplitude portion of the signal (sSSM Part 3).

Steps 2-3 each considered signals with 2 modes that were obtained by superposing the responses from two uncoupled SDOF Iwan oscillators together. The only difference between steps 2 and 3 was the separation between the modes' natural frequencies. Step 2 contained two distant modes separated by 101 Hz, while step 3 had closely spaced modes separated by just 4.1 Hz. Most of the methods tested in this work had proved effective in finding the frequency and damping for signals similar to steps 0-2. They had not, however, been proven to distinguish between two modes that were close in frequency. As mentioned in Section 2.1, at least one of three filtering methods had to be applied to multi-harmonic responses so that the mono-harmonic methods could be utilized. For step 2, both EFD and a 3rd order Butterworth filter with Matlab's `filtfilt` function were utilized to extract a mono-harmonic response before applying the Hilbert transform. The SSM-ROMs, meanwhile, were only derived using data obtained by applying a Butterworth filter. The results of each method on step 2 can be seen in Fig. 9.

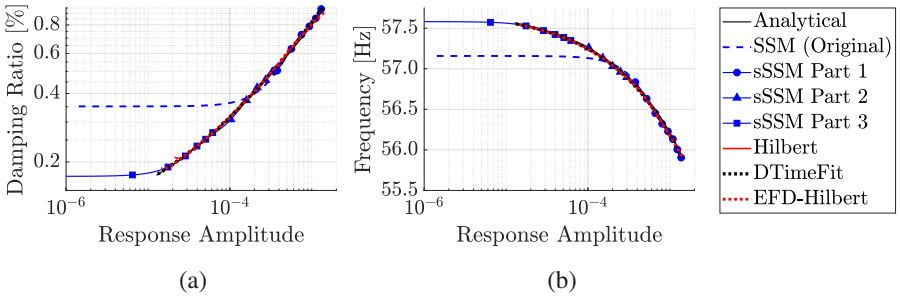

Figure 8: Step 1 damping ratio (a) and natural frequency (b) computations for the 1 DOF nonlinear response produced from an Iwan element. All methods performed well, except for the single SSM-ROM produced by the "SSM (Original)" method, which became inaccurate at low amplitudes."sSSM Part 1", "sSSM Part 2", and "sSSM Part 3" refered to the three different ROMs that were computed from the split response in the "sSSM method." The response amplitude shown in this plot was again physical amplitude.

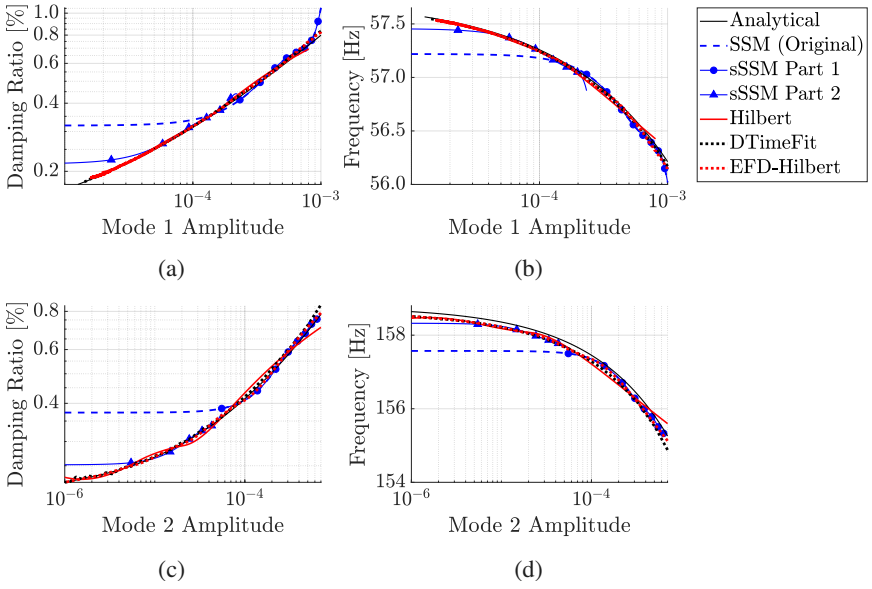

Figure 9: Step 2 damping ratio (a) and natural frequency (b) computations for mode 1 of the 2 DOF nonlinear response with distant modes created from two uncoupled Iwan elements. The bottom two panels show the damping ratio (c) and natural frequency (d) for mode 2. Once again, all methods performed well except the original SSM method, which fit a single ROM to the entire response, and the "sSSM method," which was not quite able to resolve the error at low amplitudes with two ROMs. The amplitudes shown in this plot were physical amplitudes of each mode.

A similar pattern from step 1 was again present in step 2 in Fig. 10, and all of the methods were able to extract the natural frequency and damping content at high amplitudes. However, fitting a single SSM to an entire modal response produced inaccuracies at low amplitudes because the high-amplitude data biased the fit of the model. As shown by the results for sSSM Part 2, the low-amplitude errors decreased substantially when a ROM was fit to just the low-amplitude data. The results for SSMs could have improved even more with further adjustments to the fitting parameters in SSMLearn.

The results from step 3 of this comparison study deviated the most from any of the previous steps. As shown in Fig. 10, each method differed from the analytical solution for both modes. The two methods that most accurately captured the frequency and damping from the signal were the Direct Time Fitting Method, and the Hilbert Transform after applying a 3rd order Butterworth filter with cutoff frequencies at 55.5 Hz and 58 Hz to isolate mode 1, and cutoff frequencies at 58 Hz and 62.5 Hz to isolate mode 2.

After each method was applied to a signal, the root-mean squared percent error (RMSPE) was calculated to compare the accuracy of each method in generating backbone curves. First, the RMSPE for frequency was computed using

$$\varepsilon_\omega = \text{RMS}\left(\frac{\omega_{\text{analytical}} - \omega_{\text{extracted}}}{\omega_{\text{analytical}}} \times 100\%\right). \tag{14}$$

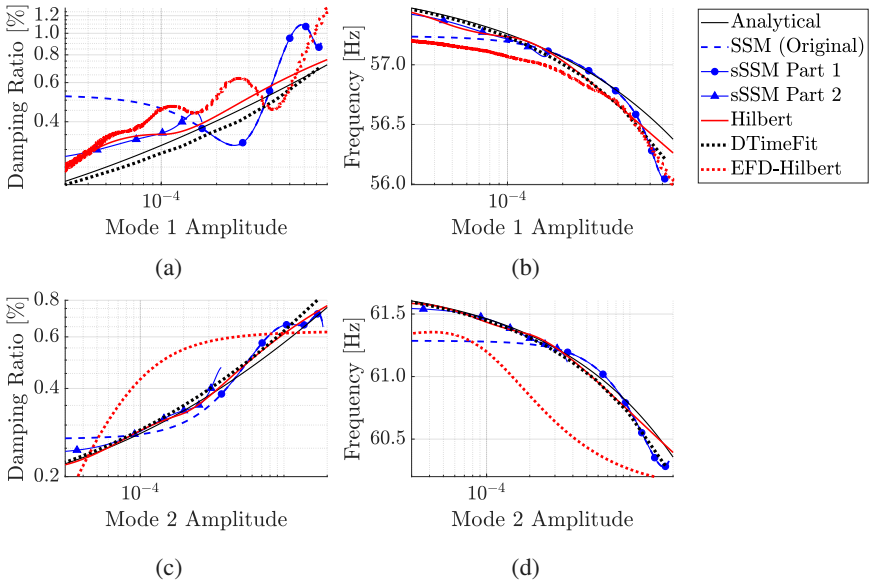

Figure 10: Step 3 verification results for the 2 DOF nonlinear response with close modes. The top two panels show the damping ratio (a) and natural frequency (b) of mode 1, and the bottom two panels show the damping ratio (c) and natural frequency (d) for mode 2. All of the methods except DTimeFit and the original "Hilbert" method with a bandpass filter exhibited spurious oscillations in damping.

Similarly, the RMSPE for the damping was found using

$$\varepsilon_\zeta = \text{RMS}\left(\frac{\zeta_{\text{analytical}} - \zeta_{\text{extracted}}}{\zeta_{\text{analytical}}} \times 100\%\right) \tag{15}$$

The final error metric used to assess a method's accuracy was given by

$$\varepsilon_T = \sqrt{\varepsilon_\omega^2 + \varepsilon_\zeta^2} \tag{16}$$

The RMSPE for every mode in each step was then compared, along with the time that was needed to run each method. As shown in Fig. 11, Direct Time Fitting produced the most accurate backbone curves in the shortest amount of time. It was believed that providing the gradient of the cost function for DTimeFit was the main reason for its short run times. It should also be mentioned that DTimeFit was able to solve for the frequency and damping of both close modes from Step 3 simultaneously, as the optimization could be used to fit multi-harmonic responses. However, much time was spent fine-tuning the window sizes for Direct Time Fitting before the result in Fig. 10 was obtained. If too small of a window was used, it was possible that a window would not capture a full cycle of the signal, and give erroneous results. On the other hand, if too large of a window size was used then the initial assumption that the response was short enough in each window to be considered linear was incorrect. In this case, a linear analytical signal could not be fit to the response encapsulated by the large window.

The high accuracy of the original SSM method for mode 2 of the close mode response occurred because of its accurate reconstruction of the damping curve. Since damping was four orders of magnitude smaller than frequency, the small value of $\zeta_{\text{analytical}}$ in the denominator in Eq. 15 caused ε_ζ to dominate in the computation of ε_T. Since the SSM (Original) curve remained near the analytical damping curve in Fig. 10(c), the SSM (Original) method ended up having a relatively low error in Fig. 11 for close mode 2. It should also be mentioned that even though SSMLearn required the longest run times, it was the only method that could create a reduced-order model that could be integrated to predict system response to different initial conditions and forcing. Also, the higher RMS error with the original SSM method was substantially reduced when SSM-ROMs were fit to the low amplitude data in the "split SSM method." Fitting an SSM using high-amplitude data was something that was experimented with in this study, but was not the intended application of SSMLearn [3].

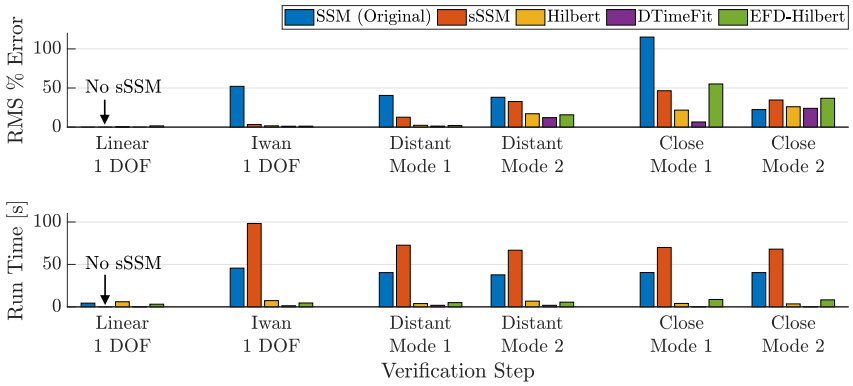

Figure 11: Summary of the performance of each method on the verification data, in terms of error (ε_T) in capturing the damping and natural frequency curves and in run time. Since a single SSM-ROM generated accurate backbone curves on the linear 1 DOF response (step 0), there was no need to split the response and fit multiple ROMs.

4 Results on Experimental Data

After comparing the methods' performance on the analytical signals in Section 3, they were each applied to experimental data without an analytical solution. This 'black box' data was collected in January 2023 on a 22" $\times$ 16" airplane-like model shown in Fig. 12 made from bolted metal plates. Due to the symmetry present in the model, it was expected that closely spaced modes would be present in the response of the system, making it a desired subject for this work. Responses from this structure were collected using 26 triaxial accelerometers and 17 uniaxial accelerometers, resulting in 95 DOFs. Nonlinear time series data was obtained from 4 drive points and 31 impacts at varying force levels, and the data from accelerometer 105Z was specifically used in the present study. For more information on the testing methods used to extract the linear and nonlinear responses of the system, see [22]. After examining the FFT of the responses, it was clear that modes 2 and 3 were the most pertinent modes to this work due to their small, 1.4 Hz difference in frequency. It should be noted that this difference in closely spaced modes was relative, as in other systems, an absolute difference of 5 Hz could be close. To further visualize the frequency content of modes 2 and 3, the FFT of the time response at DOF 15 was included in Fig. 13. Representations of the mode shapes for modes 2 and 3 were also included in Fig. 13(b)-(c).

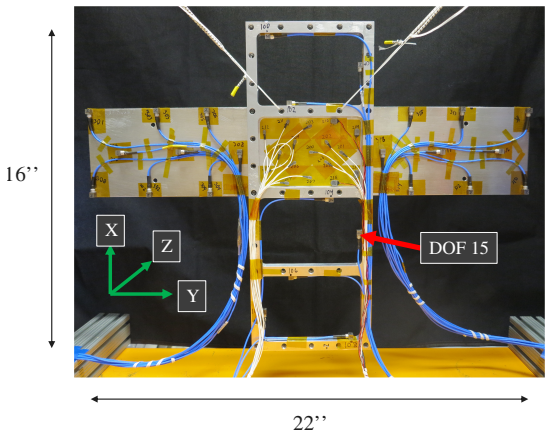

Figure 12: Experimental airplane used as the 'black box' structure. The location of the 15th degree of freedom is marked to compare the mode schematics in Fig. 13(b)-(c) with the physical shape of the structure.

The results of the analysis methods on modes 2 and 3 are given in Fig. 14. Although none of the methods agreed perfectly on the damping ratio and natural frequency of mode 2 in Fig. 14(a)-(b), they still exhibited the same trend. The natural frequency decreased at low amplitudes, indicating a softening nonlinearity, before increasing at higher amplitudes, indicating a hardening nonlinearity. Accordingly, the damping ratio initially decreased, before increasing at modal amplitudes greater than 30.

As seen in Figure 14, the Hilbert transform applied with EFD (EFD-Hilbert), the Hilbert transform applied with a Butterworth filter (Hilbert original), and DTimeFit produced the smoothest trends for mode 2. A single SSM-ROM (SSM original) also produced smooth trends, but varied from the damping ratio trends observed by the other methods at low amplitudes. The "split SSM method," on the other hand, agreed with the other methods' damping estimates, but exhibited oscillations in frequency that

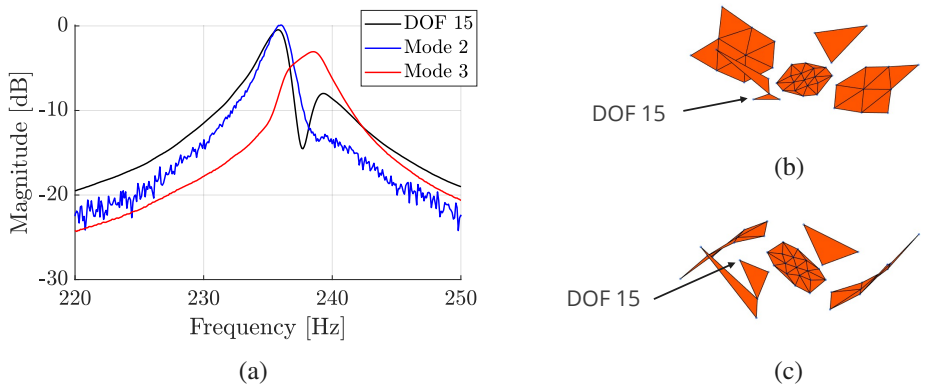

Figure 13: (a) FFT of modes 2-3 from the experimental wing, which were spaced 1.4 Hz apart. The two modal responses used to create these curves were obtained using a modal filter. Also, the FFT of the time response at DOF 15 is shown to further visualize the two close modes. Snapshots of mode 2 (b) and mode 3 (c) in motion are included as well.

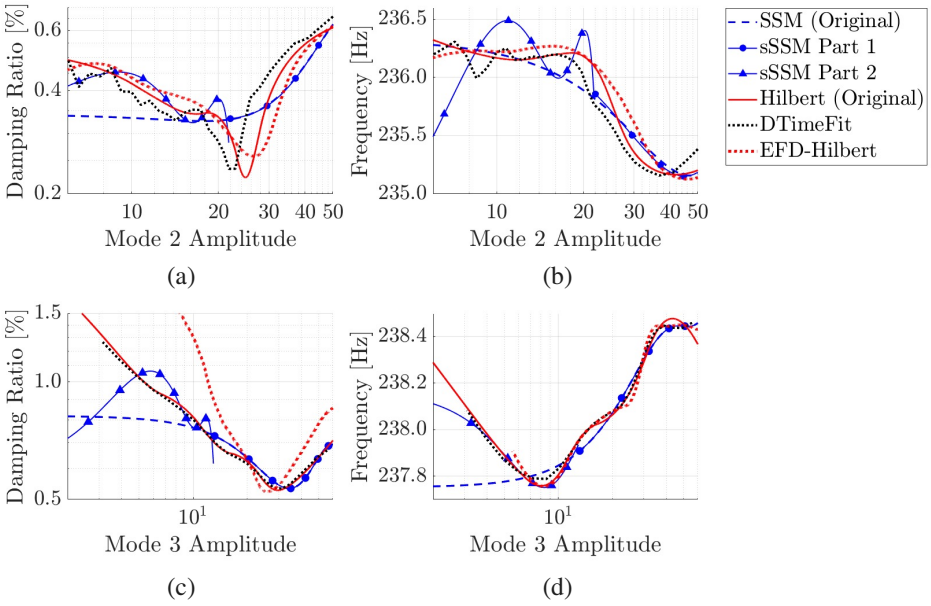

Figure 14: Damping ratio (a) and natural frequency (b) for mode 2 of the experimental data, along with damping ratio (c) and natural frequency (d) for mode 3. The amplitudes shown in this plot are mass-normalized modal amplitudes.

were caused by poor fitting. This likely occurred because the low amplitude portion of the response was too short for SSMLearn to process on its own. This meant that a ROM tuned to higher amplitudes fit to be used to approximate lower amplitudes.

For mode 3 in Fig. 14, the original Hilbert transform method with a Butterworth filter agreed with DTimeFit, but the other methods differed, especially at modal amplitudes less than 10^1. These inconsistencies were again most likely caused by fitting errors on the low amplitude portion. It can be noted that mode 3 had smaller amplitudes than mode 2, which made it more difficult to capture its frequency and damping content. The methods also showed a softening and then hardening in the natural frequency for mode 3. This behavior was due to the multi-directional loading of the joint caused by the modal response of the system, leading to non-monotonic behavior in the backbone curves.

5 Conclusion

This study compared three approaches for analyzing nonlinear systems: the Hilbert transform, Direct Time Fitting, and spectral submanifold reduced-order modeling. These approaches were used in conjunction with three different filtering techniques, including a modal filter, a 3rd order Butterworth bandpass filter, and empirical Fourier decomposition. The performance of

the methods was first quantified on four analytical signals with known frequency and damping solutions, before each method was applied to an experimental problem with no reference solution. For the analytical mono-harmonic signals in Figs. 7-8 and the analytical signal with distant modes in Fig. 9, the Hilbert transform could produce accurate backbone curves as long as unphysical oscillations were avoided by decreasing the number of knots used in the spline interpolation of the amplitude envelope. As demonstrated in Fig. 11, the Direct Time Fitting method could run faster than the Hilbert transform and produce consistently accurate backbone curves. Meanwhile, the SSM approach had the unique capability of producing a differential equation that could be integrated to simulate responses to unseen initial conditions or forcing. This was a significant advantage that set SSMs apart from the other methods. Furthermore, SSM-ROMs could create accurate backbone curves as long as they were fit to the low-amplitude portions of responses. If SSMs were fit to the high-amplitude portions of the nonlinear analytical signals, errors developed because SSMLearn was trying to fit non-polynomial dynamics with polynomials. For the experimental data, effects from higher-order modes or noise could also be present during the early parts of responses that needed to be trimmed away in order to produce more accurate ROMs.

There are areas in which all of the methods used in this study can improve. Although Direct Time Fitting was quick and effective, it was difficult and time-intensive trying to adjust the window size and window overlap ratios in order to produce the most accurate results. SSM-ROMs, meanwhile, are powerful tools that have applications beyond the scope of this study. However, this investigation demonstrated the risks of fitting SSMs to high-amplitude data and showed that the most accurate results came when SSMs were just fit to the low-amplitude portions of signals. Another possible challenge with fitting SSM-ROMs is that sometimes the eigenvectors making up a linear eigenspace are non-normal, which makes orthogonal projections onto eigenspaces less accurate than oblique projections. Future work will redo the SSM analysis on the same data from this study by considering oblique projections. A further goal for future SSM investigations is to fit ROMs to low-amplitude data and then integrate them to see how well they predict the high-amplitude data. Doing this was possible in the present study, but a priority was placed on comparing ROMs only on the amplitude ranges they were fit to. Lastly, the empirical Fourier decomposition had difficulty on the analytical closely spaced modes signal shown in Fig. 10. Future developments could redesign EFD to accept user-inputs that specify what the mode frequencies should be in order to extract intrinsic mode functions that more authentically exhibit the frequency and damping trends of closely spaced modes.

Acknowledgements

Sandia National Laboratories is a multimission laboratory managed and operated by National Technology and Engineering Solutions of Sandia, LLC., a wholly owned subsidiary of Honeywell International, Inc., for the U.S. Department of Energy's National Nuclear Security Administration under contract DE-NA-0003525. SAND2024-13625C

References

[1] G. Kerschen, K. Worden, A. F. Vakakis, and J.-C. Golinval, "Past, present and future of nonlinear system identification in structural dynamics," *Mechanical Systems and Signal Processing*, vol. 20, no. 3, pp. 505–592, 2006.

[2] J. Noël and G. Kerschen, "Nonlinear system identification in structural dynamics: 10 more years of progress," *Mechanical Systems and Signal Processing*, vol. 83, pp. 2–35, 2017.

[3] M. Cenedese, J. Axås, B. Bäuerlein, K. Avila, and G. Haller, "Data-driven modeling and prediction of non-linearizable dynamics via spectral submanifolds," *Nature Communications*, vol. 13, Feb. 2022.

[4] S. Jain and G. Haller, "How to compute invariant manifolds and their reduced dynamics in high-dimensional finite element models," *Nonlinear dynamics*, vol. 107, no. 2, pp. 1417–1450, 2022.

[5] M. Feldman, "Non-linear system vibration analysis using hilbert transform–i. free vibration analysis method 'freevib'," *Mechanical Systems and Signal Processing*, vol. 8, no. 2, pp. 119–127, 1994.

[6] K. Worden, J. Wright, M. Al-Hadid, and K. Mohammad, "Experimental identification of multi-degree-of-freedom nonlinear-systems using restoring force methods," *The International Journal of Analytical and Experimental Modal Analysis*, vol. 9, no. 1, pp. 35–55, 1994.

[7] *Methods for the Measurement of Non-Linear Damping and Frequency in Built-Up Structures*, vol. 8: 29th Conference on Mechanical Vibration and Noise of *International Design Engineering Technical Conferences and Computers and Information in Engineering Conference*, August 2017.

[8] Q. Zhang, R. J. Allemang, and D. L. Brown, "Modal filter: Concept and applications," in *Proceedings of International Modal Analysis Conference*, pp. 487–496, 1990.

[9] W. Zhou, Z. Feng, X. Wang, and H. Lv, "Empirical fourier decomposition," 2019.

[10] A. Singh and M. S. Allen, "Simultaneous direct time fitting of a multi-mode response to determine the instantaneous frequency and damping," presented at the International Modal Analysis Conference XLI, Austin, TX, February 2023.

[11] A. T. Mathis and D. D. Quinn, "Analysis of systems with generalized light damping through method of multiple-scales with emphasis on mode-coupling," in *Proceedings of the ASME 2017 International Design Engineering Technical Conferences and Computers and Information in Engineering Conference IDETC/CIE*, 2017.

[12] M. Wall, M. S. Allen, and R. J. Kuether, "Observations of modal coupling due to bolted joints in an experimental benchmark structure," *Mechanical Systems and Signal Processing*, vol. 162, p. 107968, 2022.

[13] M. Li, S. Jain, and G. Haller, "Nonlinear analysis of forced mechanical systems with internal resonance using spectral submanifolds, part i: Periodic response and forced response curve," *Nonlinear Dynamics*, vol. 110, no. 2, pp. 1005–1043, 2022.

[14] W. Zhou, Z. Feng, Y. Xu, X. Wang, and H. Z. F. Lv, "Empirical fourier decomposition: An accurate signal decomposition method for nonlinear and non-stationary time series analysis," *Mechanical Systems and Signal Processing*, vol. 163, pp. 152–170, 2022. Recent advances in nonlinear system identification.

[15] D. P. Mandic, N. Rehman, and N. Huang, "Empirical mode decomposition-based time-frequency analysis of multivariate signals: The power of adaptive data analysis.," *IEEE Signal Processing Magazine*, vol. 163, pp. 74–86, 2013. Recent advances in nonlinear system identification.

[16] D. R. Roettgen and M. S. Allen, "Nonlinear characterization of a bolted, industrial structure using a modal framework," *Mechanical Systems and Signal Processing*, vol. 84, pp. 152–170, 2017. Recent advances in nonlinear system identification.

[17] B. J. Moldenhauer, *Nonlinear System Identification Methods for Characterizing Amplitude Dependent Modal Properties*. PhD thesis, University of Wisconsin - Madison, 2022.

[18] G. Haller and S. Ponsioen, "Nonlinear normal modes and spectral submanifolds: Existence, uniqueness and use in model reduction," 2016.

[19] M. Jin, G. Kosova, M. Cenedese, W. Chen, A. Singh, D. Jana, M. R. Brake, C. W. Schwingshackl, S. Nagarajaiah, K. J. Moore, and J.-P. Noël, "Measurement and identification of the nonlinear dynamics of a jointed structure using full-field data; part ii - nonlinear system identification," *Mechanical Systems and Signal Processing*, vol. 166, p. 108402, 2022.

[20] Z. Xu, B. Kaszás, M. Cenedese, G. Berti, F. Coletti, and G. Haller, "Data-driven modelling of the regular and chaotic dynamics of an inverted flag from experiments," *Journal of Fluid Mechanics*, vol. 987, p. R7, 2024.

[21] D. J. Segalman, "A Four-Parameter Iwan Model for Lap-Type Joints," *Journal of Applied Mechanics*, vol. 72, pp. 752–760, 02 2005.

[22] "Round Robin Frame Structure," Dynamic Substructuring Focus Group Wiki. Accessed: Sep. 25, 2024. [Online]. Available: https://wiki.sem.org/wiki/Round_Robin_Frame_Structure.